Tellus (2008), 60A, 411–426
Printed in Singapore.

TELLUS

Response in extremes of daily precipitation and wind from a downscaled multi-model ensemble of anthropogenic global climate change scenarios

By JAN ERIK HAUGEN[1]* and TROND IVERSEN[1,2], [1]*The Norwegian Meteorological Institute, P.O. Box 43 Blindern, 0313 Oslo, Norway;* [2]*Department of Geosciences, University of Oslo, Norway*

(Manuscript received 3 May 2007; in final form 3 January 2008)

ABSTRACT

Time-slices of eight global climate model (GCM) response simulations of the IPCC IS92a, CMIP2, SRES A2, B2 and A1B greenhouse gas scenarios have been downscaled using the HIRHAM atmospheric regional climate model (RCM). The area covers Central and Northern Europe, adjacent sea-areas and Greenland. The GCM data were provided from the Max Planck Institute, Germany (MPI), the Hadley Centre, U.K. (HC), the Bjerknes Centre, Norway (BCCR) and University of Oslo, Norway (UiO). The resulting ensemble covers a range of future climate realizations from different global models, different greenhouse gas scenarios and natural climate variability. In order to present trends in statistical parameters including extreme events and their return periods, the downscaled response data are combined as an ensemble of equally valid possible realizations. The combined statistics is obtained after adjustments accounting for (i) different set-ups of the respective GCMs in producing the control climate and (ii) the variable range of time between the control and scenario periods. We find that annual extreme events of daily precipitation and wind speed in the control climate become more frequent in the scenario period over large areas in Northern Europe. The variability in the regional result appears sensitive to the phase of the Scandinavian pattern.

1. Introduction and background

Scenarios for the development of the global climate as a consequence of presumed atmospheric concentration levels of anthropogenic (and natural) greenhouse gases are based on coupled global climate models (GCMs) with coarse atmospheric horizontal grid-resolution (typically ~280 km or T42). For most environmental impact studies this resolution is far too coarse. Topography and patchy geographical features, such as coastlines, snow-cover, vegetation, watersheds etc., are too coarsely represented for a direct quantification of impacts of societal or ecological importance. Furthermore, features associated with atmospheric dynamics and physics are also crudely represented. For extreme weather such as strong winds and heavy precipitation, horizontal resolution is important. Such events are frequently connected with spatially abrupt features like sharp fronts and squall lines, meso-scale vortices and steep mountain slopes. Hence, an analysis of potentials for anthropogenic change in occurrence withextreme weather can not fully rely on raw output from GCMs.

*Corresponding author.
e-mail: jan.erik.haugen@met.no
DOI: 10.1111/j.1600-0870.2008.00315.x

Poor representation of physical processes in the numerical models bounds the confidence in climate projections. McAveney et al. (2001) stated that AOGCM-simulations of the present climate are accurate for most variables of interest for climate change over broad continental scales seasonally and annually. These qualities deteriorate for subcontinental scales. In an attempt to palliate the coarse horizontal resolution of GCMs, different kinds of regional downscaling techniques have been developed and used over the last two decades or so (see Giorgi and Mearns, 1991 for an early review). Increased regional skill added to GCM results has been documented by atmospheric downscaling (Giorgi et al., 2001; Denis et al., 2002). Also, weather associated with fine-scale orography is better forecasted than theory for free turbulence suggests (e.g. Boer, 1994; Frogner and Iversen, 2002).

Statistical or empirical downscaling (e.g. Wilby and Wigley, 1997) has the major advantage above other techniques that a large number of global scenarios can be analysed due to low computational cost (e.g. Benestad, 2005). In such analyses, local and regional climate parameters are tied statistically to large-scale patterns resolved in GCMs. Dynamical downscaling is a physically based approach, which requires much more computer resources. This method applies in the majority of cases to atmospheric numerical models with considerably finer resolution than GCMs over limited integration domains. Such regional climate models (RCMs) can also be coupled to the ocean (e.g. Rinke et al., 2003). In most cases, as well as in this paper, the RCM is an atmospheric model which interacts with surface processes, but with prescribed ocean and sea ice state. Also, pure oceanic downscaling models are possible with atmospheric forcing prescribed from the GCM (Ådlandsvik, 2008, this issue). Sometimes dynamic downscaling is performed with global atmospheric models with higher resolution than the atmospheric component of coupled GCMs (e.g. ∼110 km or T106) with prescribed oceanic fields. Most present RCMs use horizontal resolution 20–50 km, which is still of limited usefulness for some types of impact studies. In such cases, a combination of dynamical and empirical downscaling may be a way to obtain adequate resolution (Engen-Skaugen et al., 2007). In the recent PRUDENCE-project funded by the European Union (EU), the uncertainty in the regional climate change over Europe has been addressed by a common analysis of several coordinated RCM simulations (http://prudence.dmi.dk/). A continuation and extension of this work takes place in the new project ENSEMBLES (http://ensembles-eu.metoffice.com/).

This paper is based on data from eight time-slice simulation carried out with the HIRHAM RCM for Northern Europe and adjacent parts of the North Atlantic Ocean. A comparison between the respective control and scenario climates based on monthly data is followed by a common statistical analysis by treating the data as an ensemble of equally valid realizations of the climate in the region. As demonstrated by Räisänen and Palmer (2001), the value of a multi-model ensemble is considerably larger when treated as a probabilistic forecast of climate rather. An alternative way is to construct a deterministic consensus, for example by an ensemble mean of the available model predictions. Quantifying changes in the risk of extreme events gains in particular from a probabilistic treatment (Palmer and Räisänen, 2002).

Sources of spread, and thus uncertainty, in the calculated climate projections of future climate change covered by the eight-member ensemble are: (i) different greenhouse gas scenarios; (ii) differences between the GCMs due to inaccurate knowledge and representation of processes in models; (iii) natural unforced internal variability. Räisänen (2001) estimated from 15 GCM-calculations for IPCC (2001) using the CMIP2-scenario (1% CO_2-increase per year until doubling) that regional intermodel differences dominated over internal variability. Assuming that each model's variability realistically represents the full natural unforced climate variability, the inaccurate processes in models add variability to the already simulated natural variability. In this respect model inaccuracies may yield inflated regional climate variability. However, climate models probably tend to underestimate natural climate variability, and possibly even more after dynamical downscaling with pure atmospheric RCMs (Castro et al., 2005). Since we have little reason to trust some of the GCM scenarios more than others, we stick to the common ensemble statistics. A risk is that the region's climate variability may be exaggerated when the number of participating models becomes large.

This paper's analysis addresses in particular the response in daily extreme values of precipitation and wind speed. Similar discussions based on another RCM were given by Räisänen et al. (2004) using four GCM scenarios and with different RCMs and GCMs by Christensen et al. (2001). The size of integration domains has been studied in Jones et al. (1995, 1997). The present domain is probably sufficiently small for the data imposed on the lateral boundaries to dominate the large scale. Further, it is small enough to hamper the full development of the small-scale structures. Separate tests performed by interchanging the data for sea ice and ocean surface temperature from the two driving global models, emphasize this. Hence, the RCM-results are mainly fine-scale interpretations of the global data. As discussed in Køltzow et al. (2008), this is not necessarily a benefit for the downscaled climate. Still we chose the quite small domain to keep the large-scale variability relatively unaffected.

2. Models and global forcing

The HIRHAM RCM (Christensen et al., 1997 and 1998) was imported from Max Planck Institute (MPI), Hamburg, in 1997 and a similar version has been used at the Danish Climate Centre, Copenhagen. The main components of HIRHAM are described in Bjørge et al. (2000). The model is running on a rotated spherical grid with approximately 55 km resolution. There are 19 vertical hybrid-levels (terrain-following coordinate) with $P = 0$ as the upper boundary. The integration domain covers 96×96 grid points (see Fig. 1). The physical parametrizations

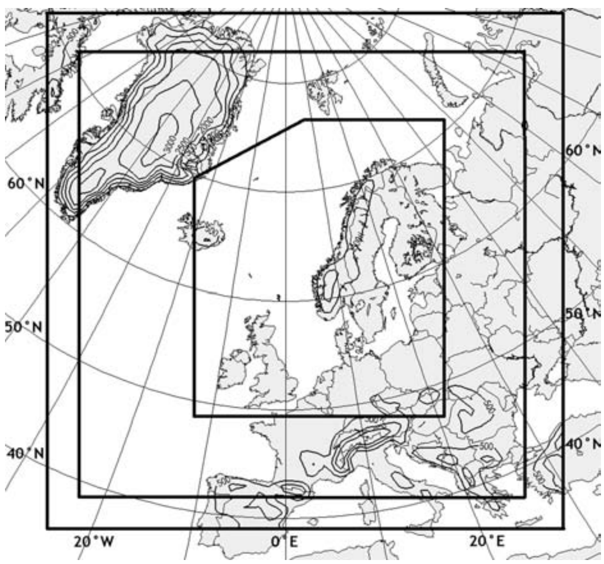

Fig. 1. The HIRHAM integration area is shown as the outer square. Most horizontal maps in this paper are displayed inside the second square, which excludes the lateral boundary relaxation zone. The inner pentagon is the area for computation of mean values used in the adjustment procedure.

Table 1. Summary of global data used as lateral and lower boundary forcing for HIRHAM RCM. There are seven different control simulations (HAD CN is common for the HC scenario periods) and eight scenario simulations. Their short names are used in the figure legends.

Centre & Model	Control	Control short name	Scenario & emission	Scenario short name	Resolution & coupling	Time-factor F(S)
MPI	1980–1999	MPI P1	2030–2049	MPI S1	T42	1.4
ECHAM4			IS92a		AOGCM	(70/50)
MPI	1961–1990	MPI CN	2071–2100	MPI B2	T106	0.636363
ECHAM4			SRES B2		AGCM	(70/110)
HC	1961–1990	HAD CN	2071–2100	HAD B2	$1.25^\circ \times 1.875^\circ$	0.636363
HadAM3H	obs. SST		SRES B2		AGCM	(70/110)
HC	1961–1990	HAD CN	2071–2100	HAD A2	$1.25^\circ \times 1.875^\circ$	0.636363
HadAM3H	obs. SST		SRES A2		AGCM	(70/110)
BCCR	30 yr	BCM E75a	Year 51–80	BCM E77	T42	1.076923
BCM v1	High AMOC		CMIP2		AOGCM	(70/65)
BCCR	30 yr	BCM E75b	Year 36–65	BCM E78	T42	1.4
BCM v1	Low AMOC		CMIP2		AOGCM	(70/50)
BCCR	1961–1990	BCM 20C	2071–2100	BCM A1B	T42	0.636363
BCM v2	20C3M		SRES A1B		AOGCM	(70/110)
UiO	30 yr	CAM CNT	30 yr	CAM CO2	T42	1.0
CAMS-Oslo	$1\times CO_2$		$1.63\times CO_2$		Slab-ocean	

are adapted from the ECHAM4 AGCM (Roeckner et al., 1996). Apart from the adaptation to different global data, the same version of HIRHAM RCM was used for all simulations in this paper. This was done in order to avoid differences due to the RCM set-up. The ocean and sea ice data in the RCM runs were prescribed from the global model runs in daily or monthly intervals.

Downscaling of the GCM data are enabled by enforcing the GCM output through the lateral and lower boundary conditions in HIRHAM. No spectral nudging is applied (von Storch et al., 2000). The different sources of GCM data are summarized in Table 1. Data from the two pure atmospheric GCMs, HADAM3H and ECHAM4 were supplied from the Hadley Centre (HC), U.K. and MPI, Hamburg, respectively. These are 30-yr long global time-slices with T106 resolution (re-runs with ocean data from the coarse resolution coupled atmosphere-ocean-sea-ice run). In the global re-run with HADAM3H the SST and sea ice were prescribed from observations for present-day period. The scenario values were then calculated from a combination of observations and the response between the control and scenario time-slices (Jones et al., 1999; Gordon et al., 2000). Data from the AOGCM run at the Bjerknes Centre, Bergen (BCCR), the BCM and from the atmospheric GCM CAM-Oslo coupled to a slab-ocean model with thermodynamic sea ice (CAMS-Oslo) supplied from University of Oslo (UiO), were also applied for downscaling. The HC-data were made available through the PRUDENCE-project, while the ECHAM4-data were kindly supplied by Dr. D. Jacob (pers. comm.). All centres, except UiO, have carried out various transient runs including recent historical periods, present day climate conditions, and future projection following the IPCC emission scenarios for the period 1990–2100.

Our experiments are based on data from five different GCMs, including two versions of the BCM, and five different greenhouse gas scenarios as detailed in Table 1. The first HIRHAM simulation with MPI ECHAM4 data was based on the old IS92a scenario designed for an earlier IPCC report. The scenario also included early estimates of the cooling effects of sulphate aerosols and stratospheric ozone reduction (Roeckner et al., 1999). The SRES B2-scenario (Nakićenović et al., 2000) assumes a gradual increase in CO_2 emissions from 7 Gt(C)/yr in 1990 to 13 in 2100, while the IS92a scenario has a slightly higher increase than the B2. The A1B has a rapid increase during the first part of the century followed by a reduction to the B2-level in 2100, and the A2 is a more extreme scenario with a steady increase to 30 Gt(C)/yr in 2100. A CMIP2 scenario assumes 1% increase in concentrations per year until CO_2 doubling in about 70 yr. The B2 scenario is a moderate scenario for greenhouse gas increase in IPCC TAR and AR4 (IPCC, 2001 and 2007).

The MPI B2 and the HC A2 and B2 data were from T106 atmospheric GCM re-runs for the two 30-yr time-slices 1961–90 and 2071–2100. Three datasets were collected from the BCM; the A1B transient scenario and two 80-yr transient CMIP2 runs. The latter two were sensitivity experiments with respect to the strength of the Atmospheric Meridional Overturning Circulation (AMOC). The global E77 and E78 BCM-simulations (with 1% increase per year in CO_2) were initiated from a year with strong and a weak AMOC meridional overturning circulation during a 300-yr BCM climate control simulation (Furevik et al., 2003; Sorteberg et al., 2005). The control climates E75a and E75b are 30-yr time-slices centred at the initial years of E77 and E78, respectively. Although, both E77 and E78 were 80-yr global simulations, the data used in the RCM were collected for years 51–80 and years 36–65, respectively. The global dataset from UiO was created by their CAMS-Oslo model, which is the NCAR CAM3 model extended with advanced aerosol physics and coupled to a slab-ocean model. CAMS-Oslo calculates the indirect and direct aerosol effects on-line with all other processes in the model and with feedback to the aerosol distribution itself (Kirkevåg et al., 2008, this issue; Seland et al., 2008, this issue). Calculations are valid for approximate radiative equilibrium at the top of the atmosphere, and thus differ from the transient data produced with the fully coupled AOGCMs. Both the control and scenario climate (with $1.63\times CO_2$ concentration approximately corresponding to doubling in a transient simulation, see Kirkevåg et al., 2008, this issue) were created by a simulated 50-yr climate equilibrium after a spin-up period of 12-yr.

In all HIRHAM atmospheric simulations, the time-slices are preceded by a spin-up period (about 1 yr) that is ignored in the analysis. This is a common procedure in RCM runs and is done mainly for adjustment of soil parameters, while for atmospheric variables a much shorter spin-up period is needed.

As always when dealing with such analyses, it is important to notice that only a subset of possible climate scenarios and climate realizations is included. Our eight simulations are certainly not sufficient to cover all natural variability and model uncertainties. On the other hand, the models show quite different regional signatures in the pressure and precipitation response over the North Atlantic–European region, see Figs. 3 and 4, and a considerable span of variability is covered. Parts of this span stem from inevitable model imperfections, but since we use the same model configuration in our regional downscaling, a large part of this spread is due to the large-scale differences in the global model data.

3. Adjustment of control and scenario climates

The 2 meter mean winter temperature responses to each GCM's radiative forcing scenarios are shown in Fig. 2. There are qualitatively large agreements between the scenarios. Two major large-scale features in the results may be seen from all the models: (1) the cold-ocean-warm-land pattern (COWL, Wallace et al., 1996; Iversen et al., 2008, this issue) is evident with considerably larger temperature increase over the European continent than over the adjacent parts of the Atlantic Ocean; and (2) the largest warming is experienced in the Arctic region. A response in the interval 2.5–4 °C is present over Central Europe and in the Nordic countries. The largest increase, more than 8 °C, in the Arctic areas is due to decreased sea ice coverage. Notice, that MPI's S1-P1 shows weaker signals than the others, since S1-P1 is only a change over a 50-yr period (1990–2040) whilst the others are over the order of 100 yrs. The 2.5 °C line along western Scandinavia can be found in most of the response maps. Differences seen over the North Atlantic Ocean during the three winter months can be associated with differences in the GCMs with respect to flow pattern trends, which also can be crudely diagnosed by the changes in mean sea-level pressure fields (MSLP).

If the COWL pattern is defined as a hemispheric pattern, it has been shown by Corti et al. (1999) to be coupled to the North Atlantic oscillation (NAO) in its positive phase. Positive NAO is associated with mild winters in Northern Europe and with large precipitation amounts over western Scandinavia. This pattern can be regarded as modulated by the more regional Scandinavian pattern originally referred to as the Eurasia-1 pattern by Barnston and Livezey (1987). A description of the pattern with seasonal maps can be found at http://www.cpc.noaa.gov/data/teledoc/scand.shtml. The main feature of this pattern is defined by an anomaly in MSLP over Scandinavia. The pattern is defined to be positive phase when the Scandinavian MSLP-anomaly is positive. Often this is an indication of an Atlantic–European blocking. In the negative phase the pattern is associated with a quasi-stationary trough over Scandinavia (e.g. Kanestrøm et al., 1985). There is some tele-connection (Wallace and Gutzler, 1981) associated with the pattern that can be seen in temperature and precipitation anomalies. The shape of the MSLP pattern and the associated precipitation and temperature anomalies vary slightly between the seasons. For Scandinavia itself, Finland and Western Russia, there is a negative correlation with the MSLP and the precipitation anomalies. Over Southern Europe, this correlation is positive, in dynamical association with the cold cyclone frequently occurring over Southern Europe during Scandinavian blocking. For the British Isles the correlation is positive in spring and autumn and negative in summer and winter. The MSLP response patterns during winter (Fig. 3) shows that the overall positive COWL trends in the scenarios are modulated differently by the Scandinavian pattern; the two MPIs show features of a positive phase, the CAMS-Oslo response a neutral phase, the BCM responses neutral and negative phases, and finally the HC responses have strong signatures of a negative phase. Associated with the Scandinavian pattern are patterns of temperature anomalies and precipitation. In short, responses with a positive trend for the Scandinavian pattern have reduced continental warming and reduced precipitation increase in Northern Europe than otherwise associated with global warming and a positive trend in COWL. These features can be recognized in Figs. 2 and 4.

The response in winter precipitation is displayed in Fig. 4. It is seen that the seasonal results depict differences with respect to the trends in the Scandinavian pattern relative to the major Scandinavian mountain ranges and coastlines. Thus there are considerable differences, which can be characterized in terms of response in MSLP and associated flow relative to the Scandinavian mountains (Fig. 3). For example; with an increased cyclonic activity in southern Scandinavia and in the northern parts of Continental Europe, in line with a negative Scandinavian pattern, HAD B2 projects increased winter precipitation in Central Europe and South and south-east of the Scandinavian mountains. Consistent with this, precipitation decreases over North-Western and northern Norway. With MPI B2, however, less cyclonic activity takes place in southern Scandinavia and more in northern Russia and Northwards, and the major winter precipitation pattern is quite opposite to that of HAD B2. Similar differences between MPI-data and HC-data were documented by Räisänen et al. (2004).

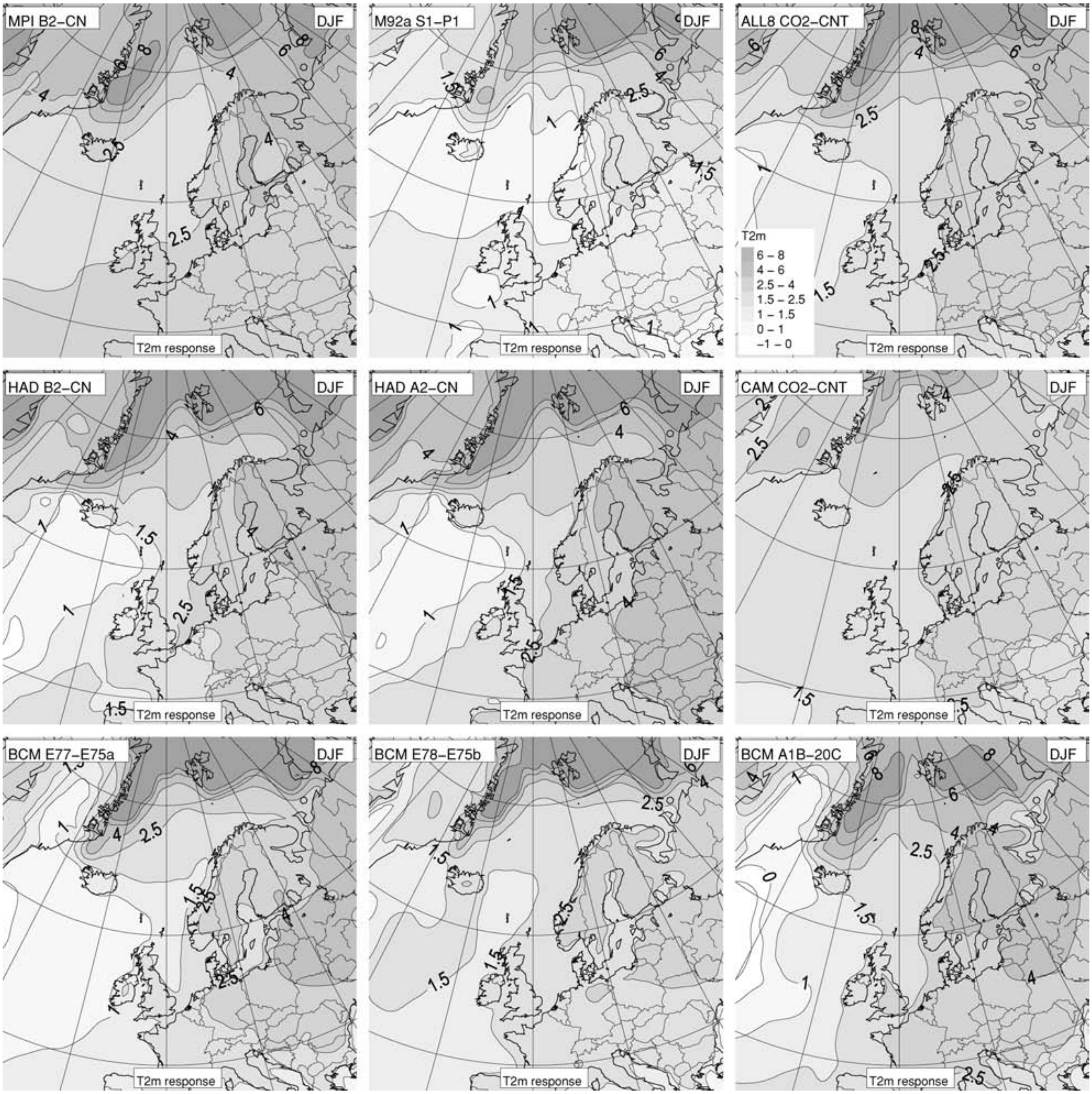

Fig. 2. The HIRHAM downscaled winter (DJF) temperature response (°C). See Table 1 for description. Lower: with BCCR data (E77-E75a, E78-E75b, A1B-20C). Middle: with HC data (B2-CN, A2-CN) and UiO data (CO2-CNT). Upper: with MPI data (B2-CN, S1-P1) and average of the eight responses (ALL8 CO2-CNT).

Since the two drastically different precipitation projections can be related to the historically observed Scandinavian flow pattern, these differences provide little objective basis for rejecting either of the two as less reliable than the other. It is plausible that the two GCMs have different error characteristics and that this contributes to artificially large spread in the combined scenario compared to natural chaotic variability. We, therefore, treat the different model-realized regional climate as not physically separable from natural variability. Consequently, the smaller internal variability in one single model (Räisänen, 2001) is interpreted as an underestimate. There is considerable uncertainty associated with this, but we treat this uncertainty as contributing to risks of occurrence of weather events. Classical results from ARCM validations (Christensen et al., 1997) show that GCMs tend to predict too much zonal displacement of cyclones over Western Europe for historical periods. The negative Scandinavian

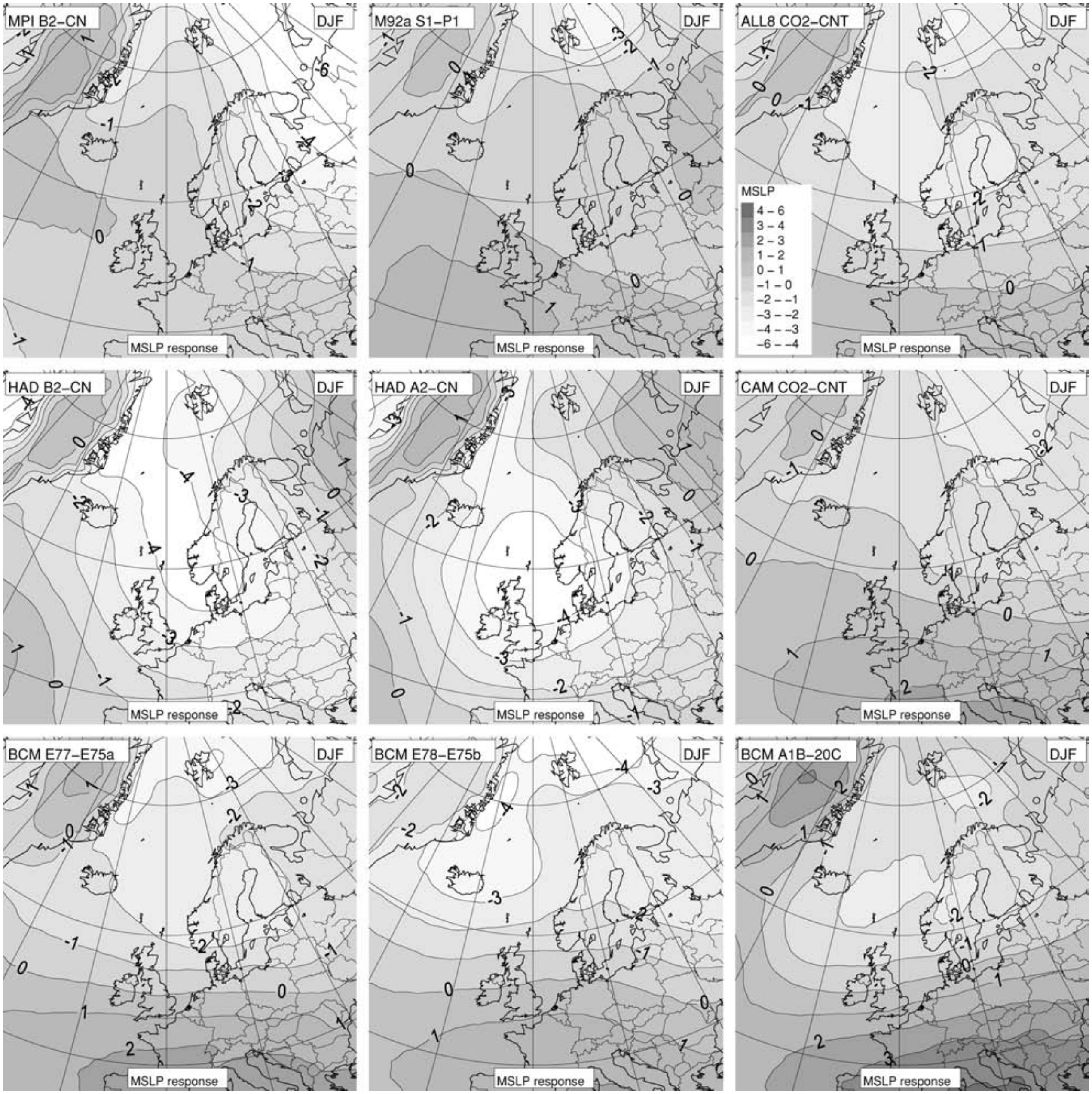

Fig. 3. As Figure 2, but for the response in mean sea-level pressure, MSLP (hPa).

pattern which appears in the averaged MSLP in Fig. 3 is possibly too strong, but this is a topic for considerable further research.

From Table 1 it is obvious that a direct comparison between the scenarios is difficult due to (i) different time-slice periods and (ii) variable set-up in the respective global models. The response periods vary between 50 yrs (MPI S1-P1 and BCM E78-E75b), 65 yr BCM (E77-E75b) and 110 yr (MPI B2-CN, HAD B2-CN and A2-CN, BCM A1B-20C). Concerning the control climates, only in the HAD CN observed sea surface temperature (SST) and sea ice coverage (SIC) are used as lower boundary forcing in the control period (1961–1990).

In Engen-Skaugen et al. (2007), the time-series of daily 2m temperatures from three of the present HIRHAM simulation were corrected by a statistical procedure. The method takes into account both differences in mean values and standard deviations compared to observed time-series at individual stations. In this study we suggest a method where the climate parameters are corrected by taking into account more regional-scale deviations between the control climates. As a diagnostic measure of 2m

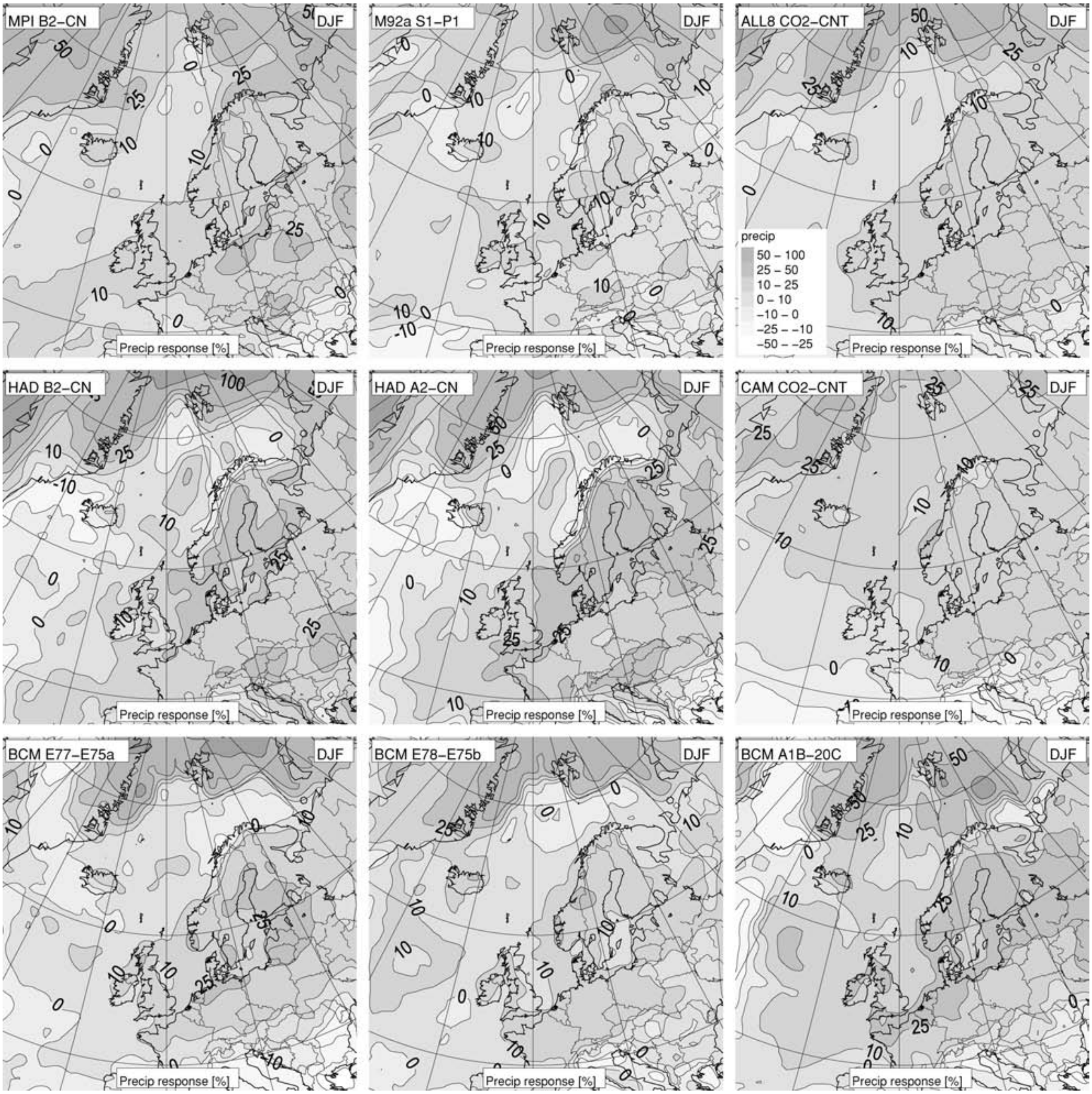

Fig. 4. As Figure 2, but for the response in daily precipitation ($mm24h^{-1}$).

temperature values, precipitation and wind speed data, monthly 30-yr mean values within the pentagon in Fig. 1 were computed for all time-slices. The subdomain covers parts of Northern Europe and adjacent sea-areas, but excludes areas with large variability and climate response due to differences in sea ice cover. The result is displayed at the first (control climates) and second (scenario climates) panel of Fig. 5 for temperature and precipitation. In the control climates, there is a central group of five time-slices and two outliers in the cold/dry and warm/moist ends, respectively. The same picture may be seen for the scenarios, but for temperature there is an additional subdivision between scenarios over different response times. The control climates in MPI P1 and MPI CN, although the data are from global coupled AOGCM simulations, have a reasonably good representation of present climate. The MPI ECHAM4/OPYC3 was shown by Allen et al. (2000) to have the best score for global climate.

Due to variable global model set-ups, in particular controlling the ocean forcing, the combination of model errors and natural climate variability leads to differences in the regional control

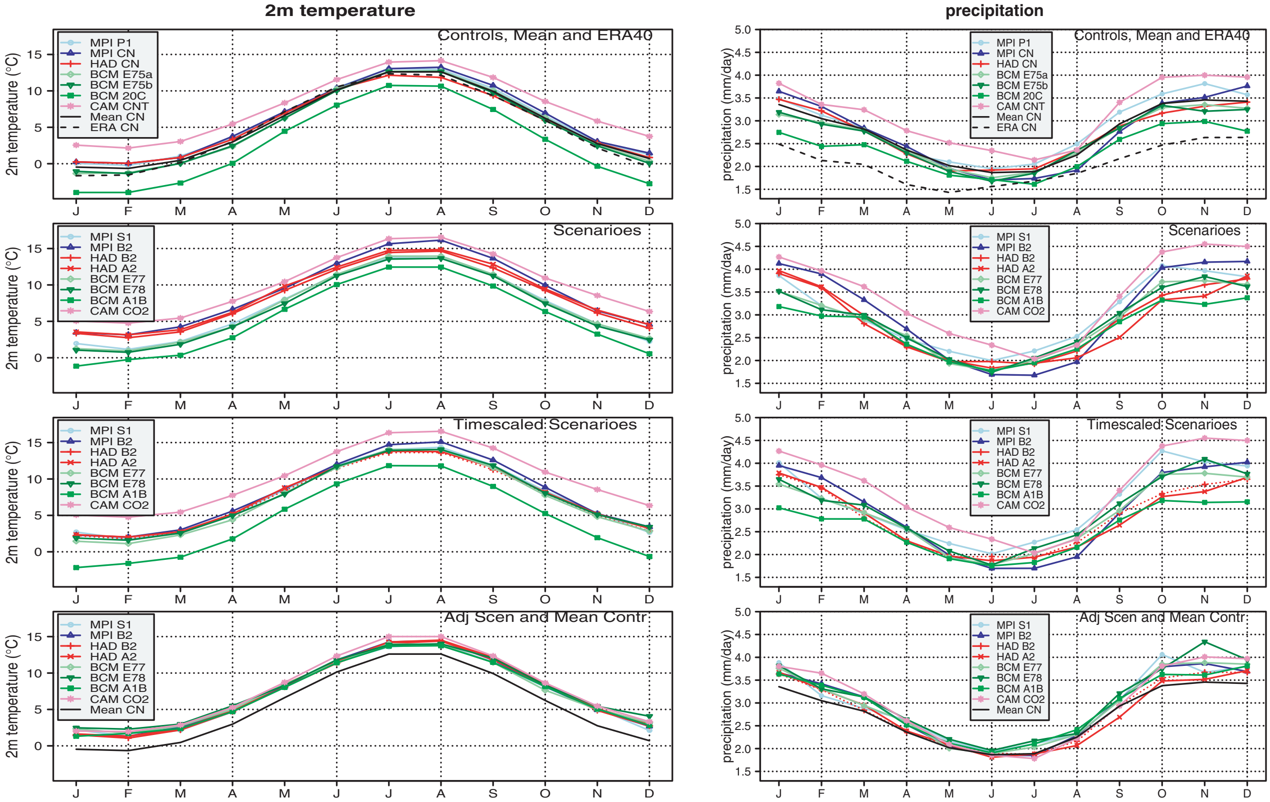

Fig. 5. Monthly means of HIRHAM 2m temperature (left) and precipitation (right) data, average values inside the pentagon area in Figure 1. From top to bottom: (i) the individual control climates, the average of controls and the corresponding ERA40 values, (ii) the individual scenario climates, (iii) the individual scenarios after correction due to difference in response time and (iv) the individual adjusted scenario climates and the mean of control climates.

climates from the global models. To compensate for these deviations we define new monthly and daily time-slice series with bias corrections of the control climates, and new scenario time-slices corrected for differences in response times between the control and scenario periods. The bias corrections are calculated from statistics over the pentagon area, and applied to 2m temperature, precipitation and wind speed. Let M denotes the monthly average value for a site or a grid-point. Then, the adjusted value M^A in the control climates and scenario climates become respectively

$$M_C^A = M_C - A_C + \bar{A}_C$$

$$M_S^A = M_S - A_S + \bar{A}_C + (A_S - A_C) \cdot F(S).$$

Here, subscripts C and S denote control and scenario, A is the pentagon area mean value of M averaged over all years within each time-slice, $\bar{A}_C$ is the average of A_C over all control climates and F(S) is the time-factor given in the right column of Table 1. We adjust the response period to be a common 70 yr for all scenarios, which is approximately the time for a CMIP2 simulation to reach the $2\times CO_2$ concentration level. Note that the CAMS-Oslo produces an equilibrium scenario at $1.63\times CO_2$ that approximately corresponds to CO_2 doubling in a transient CMIP2 scenario; hence the time factor is 1 for that model. As a result, within the pentagon, all control climates will have a mean value of $\bar{A}_C$ and each scenario climate will have the mean value $\bar{A}_C + (A_S - A_C) \cdot F(S)$. An alternative value of $\bar{A}_C$ could be computed from the ERA40 re-analysis. For temperature, it turned out that with the distribution of our control climates, the average was very close to the corresponding ERA40 value. For precipitation, and to a less extent also wind speed, the HIRHAM values were somewhat higher than the corresponding ERA40 data.

One might question whether this procedure is reasonable. The correction will limit the total variability of the model-results and potentially underestimate the contribution from the natural variability. However, when inspecting Fig. 5, it is quite apparent that the main model characteristics are maintained when comparing the curves for control and scenario periods. The model with a cold/dry control climate becomes the coldest and driest scenario. Respectively, the model with the warm/wet control climate becomes the warmest/wettest scenario (at least for the majority of the months). This is further emphasized in the third panel of Fig. 5, where the effect of time-scaling of the response, F(S), is taken into account. The separation between the scenarios looks quite similar to the controls curves, though to a higher extent for temperature than for precipitation. The two extreme outliers in the third panel in Fig. 5 are from the CAM-Oslo model (Kirkevåg et al., 2008, this issue) and the Bergen Climate Model (BCM, Furevik et al., 2003; Sorteberg et al., 2005). The reason for a warm bias in CAM-Oslo is discussed in Kirkevåg et al. (2007), and is due to an inaccurate calibration of the slab ocean model. The reason for the cold bias in the BCM is not known, but the sea-surface temperatures in the northern North Atlantic Ocean show similarities with the original HadCM3-run from the Hadley Center. From this run, without flux corrections for present climate, the data was bias-corrected in the HadAM3H atmospheric model, with corrected SST and sea ice (Jones et al., 1999).

In some way, the present procedure is similar to the visualization of global temperature during the 20th and the 21st Century in the IPCC reports (e.g. Fig. SPM-5 in IPCC, 2007). In these figures the global temperature development is compared to the global mean in 1990, a year where all models are displayed with the same global mean temperature. In reality, the deviation in the global mean of the global near surface temperature in 1990 is different from zero. In conclusion, although the procedure might limit some of the variability, we argue that it is likely that a significant part of these deviations originate from model inaccuracies. For a common analysis of the ensemble, we want to decrease this part of the error.

The resulting curves for the adjusted scenarios are displayed in the bottom row of Fig. 5 After using this filtering of systematic errors in the control climates and differences pertaining to the chosen response time between the control and scenario climates, there is a much better agreement in the response. Furthermore, a series of eight scenario climates has been obtained, which to a larger degree may justify a common analysis.

4. Combined 70-yr response in seasonal and monthly adjusted data

Before discussing the daily extremes, a common analysis of results based on monthly and seasonal values is presented. Taking into account the difference in response time, the ensemble average of the time-scaled climate responses for temperature, precipitation and wind speed is displayed in Fig. 6. (The effect of

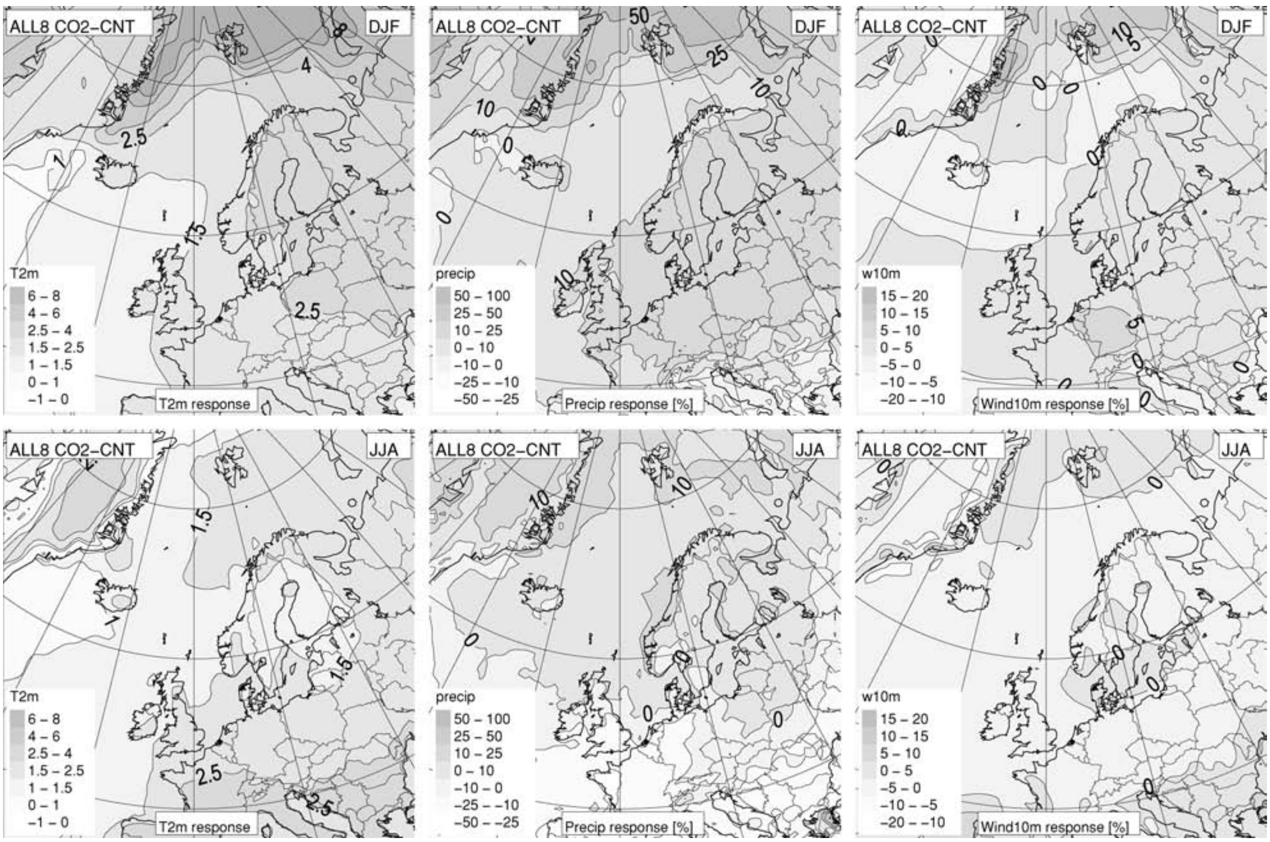

Fig. 6. Average response of the eight HIRHAM scenarios after time-scaling due to different time-slice periods. 2m temperature response in °C (left), relative precipitation response in percent (middle) and relative 10m wind speed response in percent (right). Top row is winter (DJF) and bottom row is summer (JJA).

the bias correction vanishes when looking at responses). For 2m temperature the largest warming in winter months occurs in the northern part due to feedback changes in the sea ice extent, and in northeast over continental areas in accordance with COWL. In summer the largest warming is seen in Central and Southern Europe. For winter precipitation there is a 10–20% increase in most continental areas except southern parts of Europe, while a summer drying is more evident in central and Southern Europe. In Northern Europe there is a slightly increased precipitation in summer as well, except over southern Sweden, southeast Norway and in Denmark. The average wind speed response during winter shows increased values for most continental areas with a maximum of 4% in Central Europe, and with rather small increase or a slight decrease during summer. For wind speeds caution should be taken, since high wind speeds over continents can be expected to occur on considerably smaller scales than resolved in these experiments. Furthermore, the spatial resolution we apply cannot adequately resolve features such as polar lows over open ocean during the extended winter season in the Arctic.

The climate responses at four selected Norwegian location is summarized in Table 2 for 2m temperature, precipitation and 10m wind speed. They represent different areas in Norway; Tromsø and Bergen at the west coast in north and south, respectively, are strongly influenced by the extratropical cyclones arriving over the North Atlantic Ocean and by a relative mild ocean; Karasjok is a climatologically continental site situated inland in northern Norway; and Oslo in southeast Norway is at the leeward side of the Norwegian mountains with respect to the westerlies.

For temperature there is a positive and statistically significant response at all sites and all seasons. Concerning precipitation, there is a positive mean response, except for Oslo in summer (JJA). All scenarios indicate increased precipitation from annual values, but for seasonal values and also seen from Fig. 6, we find both positive and negative responses and larger variability at regional scales. An illustrating example is Tromsø during winter where the relative response varies between −23.3% (HAD A2-CN) and +18.5% (MPI B2-CN). This difference in the regional response may be due to natural variability associated with the Scandinavian pattern; the MPI B2 scenario with an increased westerly wind forces a stronger orographic component at the west coast (positive Scandinavian pattern), while in the HAD A2 the negative Scandinavian pattern leads to decreased precipitation in the same region. Finally, for 10 m wind speed, the results indicate similar regional differences in the results from the eight scenarios as obtained for precipitation. Still, during autumn the mean response is positive (higher wind speeds) in all regions. During winter (see Fig. 6) there is a slight increase towards continental areas in Northern Europe.

Does the regional-scale adjustment procedure improve the analysis at local scales? To answer this, the distribution of monthly temperature and precipitation values were computed

Table 2. HIRHAM climate responses at four Norwegian stations; in northern part (Karasjok, Tromsø), western part (Bergen) and southeastern part (Oslo). Numbers are the mean value and in parentheses the range (min. and max.) of the eight time-scaled responses. The relative response R in% from control climate C to scenario climate S is R = (S-C)/C* 100%. Numbers appended by star indicate that the mean response is statistical significant at 95% confidence levels using Student's *t*-test.

Station	2m Temperature Months	Precipitation °C	10m Wind speed mmd^{-1}	R%	R%
Karasjok	Annual	2.8 (2.3–3.0) *	0.2 (0.1–0.3) *	10.3 (2.5–16) *	0.5 (−1.4–1.6)
	MAM	2.8 (2.2–3.3) *	0.2 (−0.1–0.3) *	10.4 (−2.9–18.5) *	0.7 (−2.1–3)
	JJA	1.8 (1.0–2.7) *	0.2 (0–0.3) *	7.8 (−0.1–12.9) *	−3 (-4.6–0.4) *
	SON	3.1 (2.2–4.2) *	0.3 (0–0.4) *	14.6 (−0.3–17.9) *	2.8 (−1.6–5.1) *
	DJF	3.5 (2.8–3.8) *	0.1 (0–0.3) *	7.8 (0.3–20.7) *	0.9 (−2–2.4)
Tromsø	Annual	2.2 (1.5–2.6) *	0.3 (0.1–0.5) *	11.1 (3–15.1) *	−0.4 (−1.7–0.8)
	MAM	2.4 (1.9–2.6) *	0.2 (0–0.6) *	9.1 (−1.2–19.9) *	−0.1 (−3.1–2.1)
	JJA	1.7 (0.9–2.7) *	0.3 (−0.1–0.9) *	10.3 (−3.5–31.5) *	−2.3 (−5.9–1.2) *
	SON	2.5 (1.6–3.2) *	0.8 (0.1–1.5) *	21.2 (2.5–39.2) *	2.1 (−3.6–4.8) *
	DJF	2.4 (1.9–3.0) *	0.0 (−0.7–0.5)	0.6 (−23.3–18.5)	−1.5 (−6.6–2.1) *
Bergen	Annual	1.7 (1.3–2.3) *	1.5 (0.4–2) *	20.1 (5.5–35.7) *	1.5 (−1.6–3.3)
	MAM	1.7 (1.3–2.2) *	0.9 (0–1.9) *	17.5 (−1–31.9) *	1.2 (−1.9–4.5)
	JJA	1.3 (0.7–2.1) *	0.7 (−0.4–1.6) *	11.0 (−7.4–32.1) *	−1.8 (−5.3–1.4) *
	SON	1.9 (1.3–2.3) *	2.2 (0.1–3.9) *	23.7 (1.1–59.1) *	2.8 (−2.7–5.8) *
	DJF	2.0 (1.2–3.1) *	2.0 (1.2–2.2) *	24.4 (12.1–32.7) *	2.6 (−0.4–5.2) *
Oslo	Annual	2.2 (1.7–2.6) *	0.3 (0.1–0.4) *	8.3 (3.9–13.9) *	0.8 (−0.8–2)
	MAM	2.0 (1.4–2.4) *	0.2 (0.1–0.5) *	8.6 (3.8–19.6) *	0.6 (0–1.7)
	JJA	1.5 (0.4–2.3) *	−0.1 (−0.8–0.3)	−4.0 (−21.9–10.4)	−1.7 (−5.9–1.7) *
	SON	2.5 (1.7–3.4) *	0.4 (0–0.6) *	9.4 (−1.1–16.1) *	1.4 (−2.6–4.4)
	DJF	2.8 (1.7–3.8) *	0.6 (0.2–1.1) *	19.9 (6.2–38.9) *	2.3 (−0.7–4.4) *

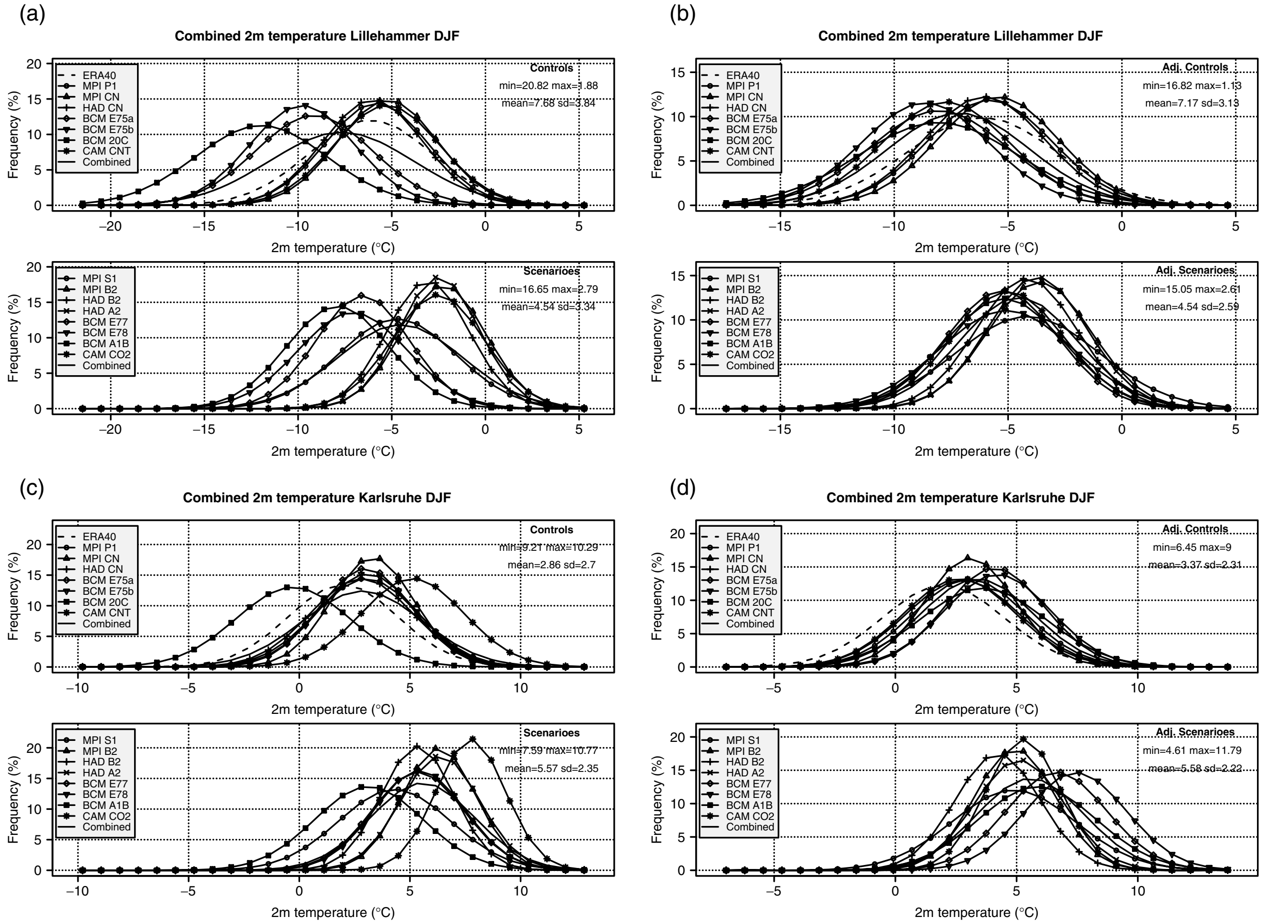

Fig. 7. Distribution of HIRHAM monthly mean winter (DJF) 2m temperatures. The curves are the Gaussian distributions of individual time-slices. Location Lillehammer (southern Norway) before (a) and after (b) adjustment, and Karlsruhe (southern Germany) before (c) and after (d) adjustment. Each subfigure shows the control climates (top) and the scenario climates (bottom). ERA40 values are included in the control figures (dashed).

for a number of different locations in Europe. Examples, for Lillehammer in southern Norway and Karlsruhe in southwest of Germany, are displayed in Fig. 7 and Fig. 8. Lillehammer is situated in the centre of the pentagon area used for computation of the difference in biases, while Karlsruhe is situated at the border of the pentagon area. For the unadjusted values, there is a 7 °C difference in the mean value between the coldest and warmest control climate and a 5 °C difference between the scenarios in Lillehammer. In the adjusted distributions, there is much better agreement at the local scale as well (about 2.5 °C difference between the coldest and warmest control) and much larger agreement between the scenario distributions. In Karlsruhe, the results for temperature in Fig. 7 are quite similar. A modified procedure was applied before adjustment of monthly precipitation and wind speed data due to skew frequency distributions with a tail towards high values. Individual monthly values were transformed with the formula $\tilde{M} = \ln(1 + M)$ that makes an approximate Gaussian distribution for $\tilde{M}$. The adjusted means were transformed back before presentation in Fig. 8. It is fair to say that the adjustment procedure works for precipitation as well. In Lillehammer the effect was quite visible, but in Karlsruhe there is minor impact after adjustment. The ERA40 temperature values show a good agreement with the HIRHAM results, but for precipitations the HIRHAM values are generally larger than computed from the ERA40 $0 + 24$ hour accumulated precipitation data. In general, the procedure improved the agreement between the different time-slices at other stations as well. The procedure increased the disagreement for precipitation and wind speed at some stations during summer, which is a season with less precipitation and wind but also with a higher influence of convective scale systems that are not resolved in the calculations.

5. Combined 70-yr response in daily precipitation and wind speed extremes

In this section the response in daily precipitation and wind speed extremes is analysed. In order to base the results on the largest possible data sample, annual extremes are presented and discussed. Analysis based on annual values may hide the fact that

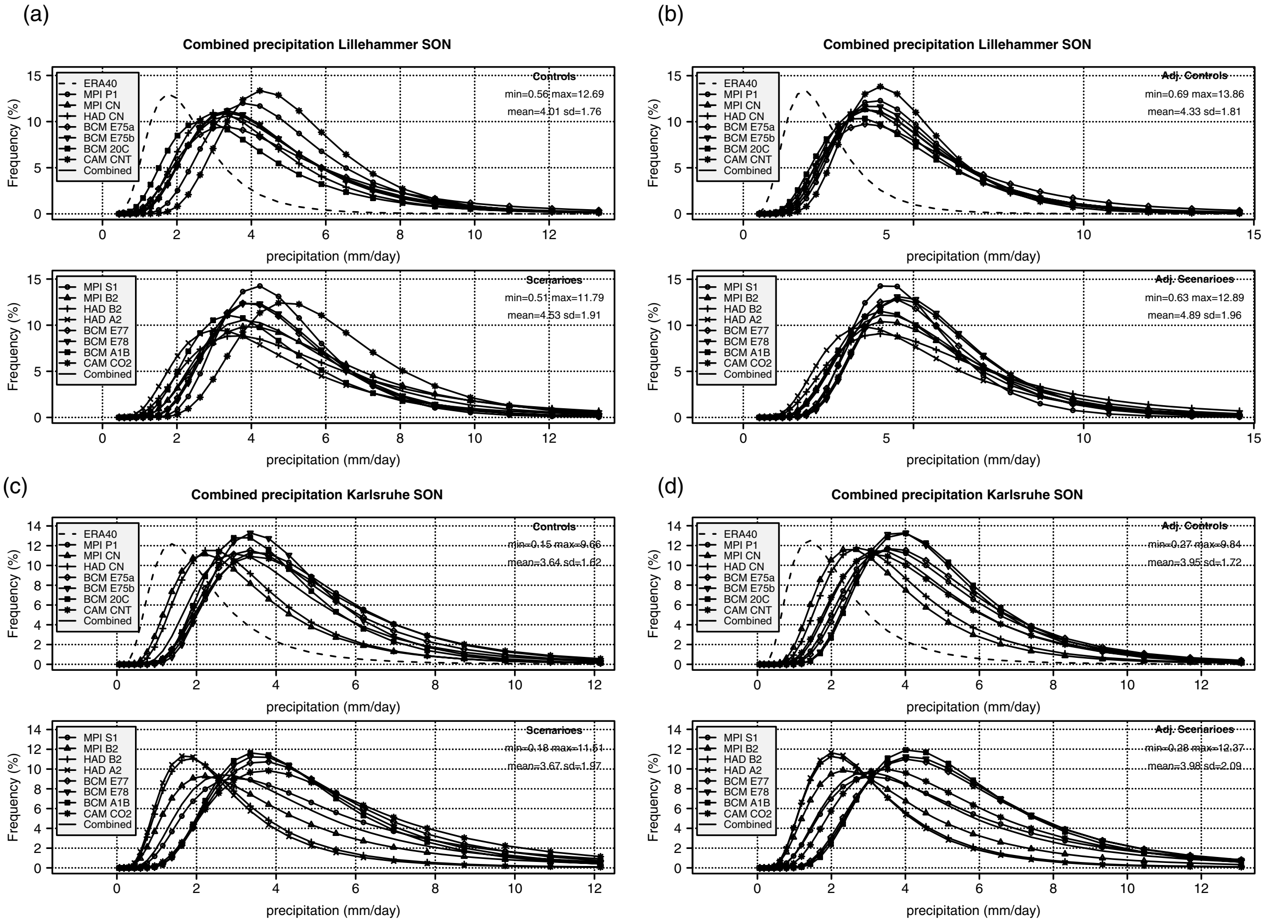

Fig. 8. As Figure 7, but precipitation. Distribution of HIRHAM monthly mean autumn (SON) precipitation. Location Lillehammer (southern Norway) before (a) and after (b) adjustment, and Karlsruhe (southern Germany) before (c) and after (d) adjustment. Each subfigure shows the control climates (top) and the scenario climates (bottom). ERA40 values are included in the control figures (dashed). Values are scaled to mmd^{-1} at the horizontal axis.

one of the scenarios may dominate the results due to large differences in the response in some periods of the year. To some extent we have corrected for this difficulty. The adjustment procedure and the results of the analysis in the previous section showed that the annual mean behaviour of the scaled scenarios is rather similar.

The statistics is computed from the time-slices in a common analysis following recommendations by Räisänen and Palmer (1991): the frequency statistics are combined to yield probabilistic measures of future climate change in the region. In the combined response statistics the datasets are given equal weights. A simple measure of changes in extreme values is the response factor (in the scenario period) of a certain high percentile as computed from the control period data. As an example, the highest 0.2778 percentile value in the control period computed from annual values corresponds to one event per year (on average). A response factor of $^1/_2$, 1 and 2, respectively, means that these values will occur with half, the same and the double frequency, respectively, in the scenario data. A statistically more robust measure, but certainly not very extreme, is the result for the highest 5 percentile, corresponding to an average occurrence of one per 18 d in the control period. Due to the relative large sample of eight scenarios, the percentile for one event per 5 yr in the control data is included. In our case, with $20 + 7\times30 = 230$ yr of control data, this corresponds to the 46 highest values.

Before analysis, the daily data were adjusted in a similar way as in Section 3. Since the adjustment was based on HIRHAM monthly mean values (or optionally ERA40 data), the adjustment should be based on the distribution of some reference dataset for daily data. The distribution of daily precipitation and wind speed data are far from Gaussian and simple correction of the mean value have very little impact on the extremes. As a simplified approach we applied a constant adjustment to the transformed series $\hat{D} = \ln(0.1 + D)$ of daily data D within a certain month. The sums of daily corrections should be equal to the previous change in monthly means. A formula where this is obtained is

$$D^A + 0.1 = (D + 0.1)\cdot(M^A + 0.1)/(M + 0.1).$$

Here, D^{A} is the adjusted daily value, and M and M^{A} must be computed from the corrections to the transformed monthly means $\tilde{M} = \ln(1 + M)$ and $\tilde{M}^{A} = \ln(1 + M^{A})$. The result gives a shift in the mean value of data with an approximate Gaussian distribution. There is an additional problem for precipitation with a separation between dry and wet days, and that for both precipitation and wind speed slightly negative values will be introduced for negative correction of the mean values. However, this is neglected, since the main interest is the high extremes. Examples of the adjustment of daily wind speed values is displayed in Fig. 9. With the present algorithm, the change in the daily distribution was in general smaller than in this example. The results for Lillehammer show that the impact is in the direction of better agreement between in both control and scenario climates. For Karlsruhe, the adjusted values show unchanged or slightly less agreement. The ERA40 data agree well with HIRHAM results at Lillehammer, in contrast to the distributions in Karlsruhe.

The scenario increase in return frequency of events for daily precipitation amounts and daily maximum wind speed are displayed respectively in Figs. 10 and 11. The results show some similarities. For both parameters the return factors mainly are higher than 1, meaning increased occurrence. The factors increased further for gradually more extreme events. The highest factor for the 5%tile of precipitation exceeds 1.25 in Northern Europe; the 1 per year occurrence has a return factor higher that 1.5 in major parts of the area, while the 1 per 5-yr event will occur twice as often in many areas. For maximum daily wind speed the highest return factors are limited to the eastern part of the domain, reaching the same values as for precipitation except for the highest 5%tile, which does not exceed 1.25. Similar fields were also computed for unadjusted parameters, and the results were rather similar. The largest difference was found for wind speed, where the return factor for the highest extremes was slightly larger for the adjusted data. The spatial

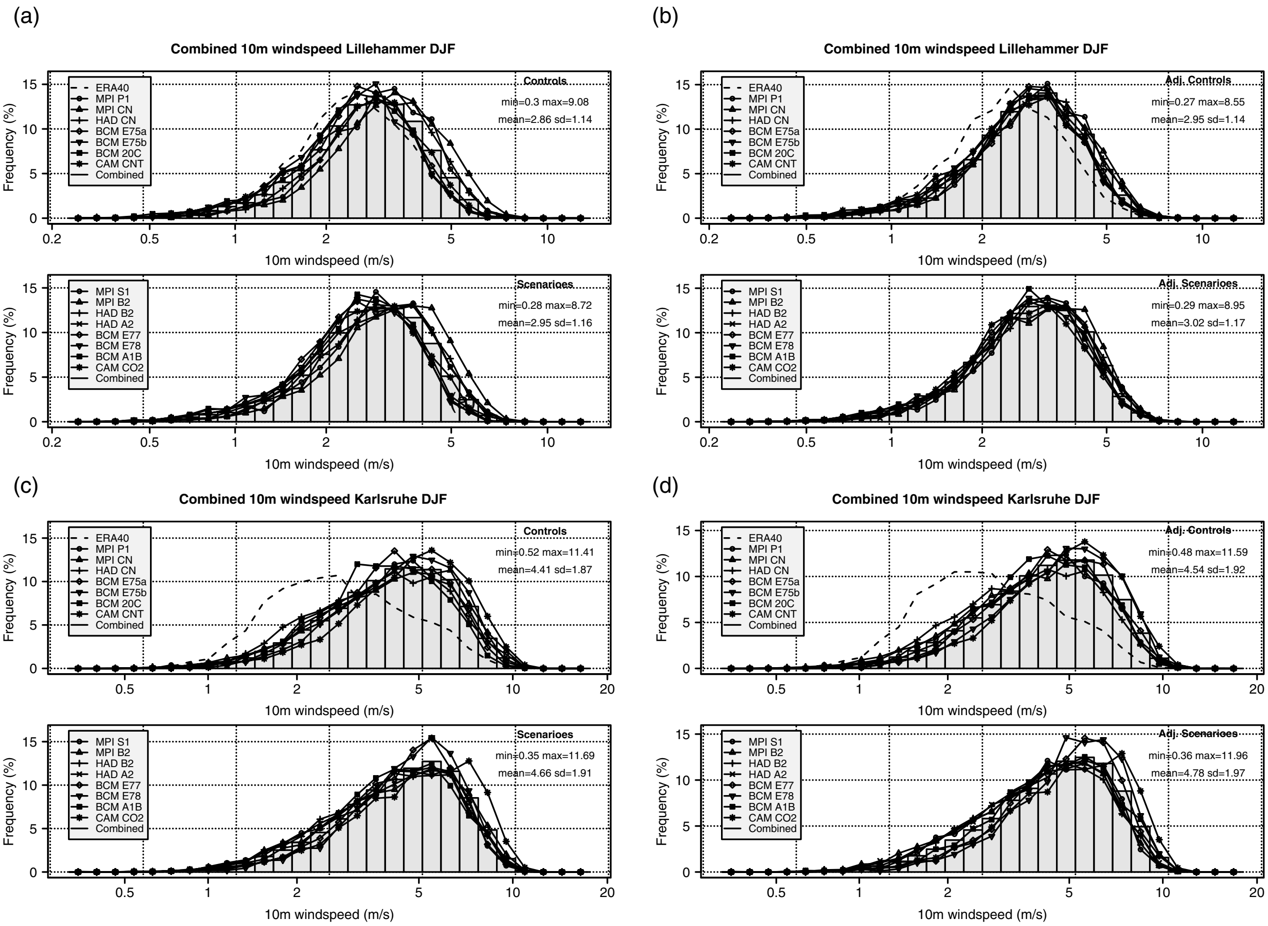

Fig. 9. Distribution of HIRHAM daily 10m maximum wind speed data for winter months DJF. Gray bars is the histogram of all daily values, and the curves are data from individual time-slices. Location Lillehammer (southern Norway) before (a) and after (b) adjustment, and Karlsruhe (southern Germany) before (c) and after (d) adjustment. Each subfigure shows the control climates (top) and the scenario climates (bottom). ERA40 values are included in the control figures (dashed). The horizontal axis is transformed to ln(x+0.1), but labels are as untransformed values (ms^{-1}).

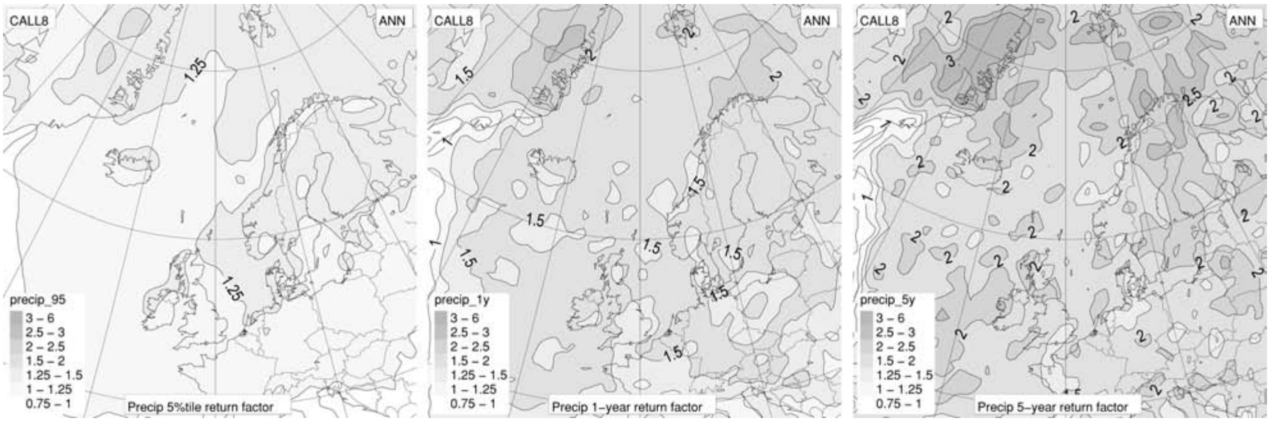

Fig. 10. Return factor of daily precipitation values from combined analysis of the eight HIRHAM scenarios, based on adjusted data. The three maps are computed from different percentiles in the control climate; the highest 5% percentile (left), and the percentiles corresponding to 1 per year occurrence (middle) and 1 per 5-yr occurrence (right). A return factor of 2 means twice as often.

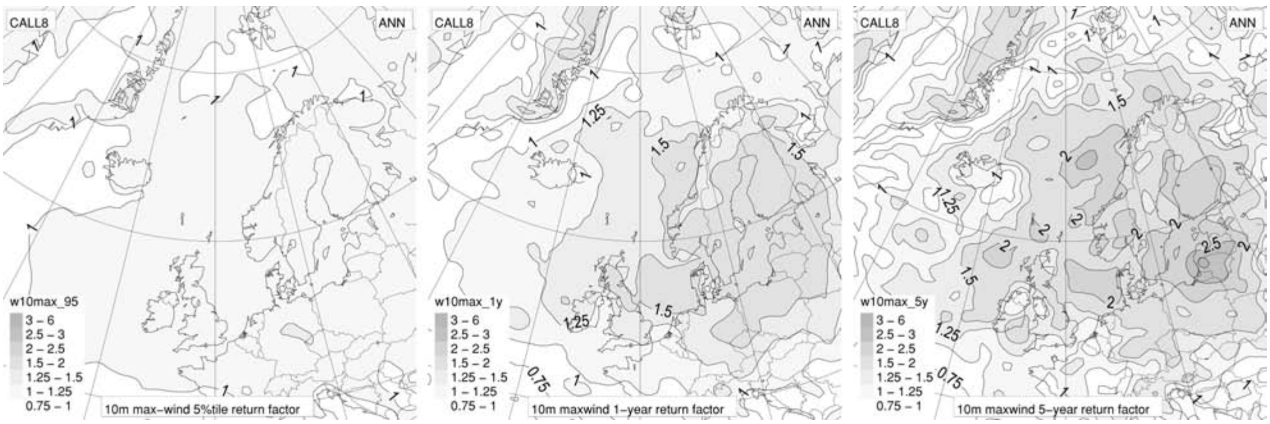

Fig. 11. As Fig. 10, but wind speed. Return factor of daily 10 m maximum wind speed data from combined analysis of the eight HIRHAM scenarios, based on adjusted data. The three maps are computed from different percentiles in the control climate; the highest 5% percentile (left), and the percentiles corresponding to 1 per year occurrence (middle) and 1 per 5-yr occurrence (right). A return factor of 2 means twice as often.

pattern of increased return frequency bears resemblance with the patterns of the mean responses found in the winter responses in Fig. 6.

6. Conclusions

The paper discusses some selected results from dynamical downscaling over Europe and adjacent sea areas using a frozen version of the HIRHAM RCM. Eight global realizations of the climate response with five global model versions and at least five different emission-scenarios were downscaled. Concerning response in mean fields, the largest warming during winter occurs in Northern Europe. Central and Southern Europe experience the largest warming during summer, associated with a drier climate. Precipitation response during winter is positive over major parts of Europe, but with regional differences coupled to different trends in the atmospheric circulation between the scenarios appearing as different phases of the Scandinavian pattern. To account for differences in the control climates of the respective global models and differences in the response periods, an adjustment procedure was suggested and applied. The adjustment decreased the regional-scale difference due to, for example variations in the set-up of the global models and large-scale model errors, thus giving a more consistent set of scenario climates for analysis of extremes.

The return factor for moderately extreme daily events of precipitation and wind speed follows to a large extent the patterns seen in the mean response. The response in return frequency for more extreme events is estimated to be considerably larger than for moderate high percentiles. Still, parts of the results may be caused by errors in the model results due to model imperfections. By including an even larger number of climate realizations more robust estimates should be obtained. Two subjects for further research are (i) to what extent the different responses in regional flow patterns over Northern Europe are equally realistic realizations of natural variability and (ii) whether a strengthening of a negative phase Scandinavian pattern during global warming is realistic.

7. Acknowledgment

The work reported here is funded in part by the Norwegian Research Council, through grant no. 120656/720 to the Norwegian Meteorological Institute/RegClim. Computational costs are covered by a grant from the Research Council's Programme for Supercomputing. The Hadley Centre, the PRUDENCE project at the Danish Climate Centre, the staff at MPI (Dr. Daniela Jacob), BCCR (Dr. Frode Flatøy) and UiO (Dr. Alf Kirkevåg) are gratefully acknowledged for support of the global data. We thank two anonymous reviewers for their helpful comments.

References

Ådlandsvik, B. 2008. Marine downscaling of a future climate scenario for the North Sea. *Tellus* **60A**, doi:10.1111/j.1600-0870.2008.00311.x.

Allen, M. R., Stott, P. A., Mitchell, J. F. B., Schnur, R. and Delworth, T. L. 2000. Quantifying the uncertainty in forecasts of anthropogenic climate change. *Nature* **407**(Oct. 5), 617–620.

Benestad, R. E. 2005. Climate change scenarios for Northern Europe from multi-model IPCC AR4 climate simulations. *Geophys. Res. Lett.* **32**, L17704, doi:10.1029/2005GL023401.

Bjørge, D., Haugen, J. E. and Nordeng, T. E. 2000. Future climate in Norway. *DNMI Research Rep*. **103**, 41 pp. Norwegian Meteorological Institute, P. O. Box 43 Blindern, N-0313 Oslo, Norway, ISSN 0332-9879.

Boer, G. J. 1994. Predictability regimes in atmospheric flow. *Mon. Wea. Rev.* **122**, 2285–2295.

Barnston, A. G. and Livezey, B. E. 1987. Classification, seasonality and persistence of low-frequency atmospheric circulation patterns. *Mon. Wea. Rev* **115**, 1083–1126.

Castro, C. L., Pielke, Sr., R. A. and Leoncini, G. 2005. Dynamical downscaling: Assessment of value retained and added using the Regional Atmospheric Modeling System (RAMS). *J. Geophys. Res.* **110**, D05108, doi:10.1029/2004JD004721.

Christensen, J. H., Machenhauer, B., Jones, R. G., Schär, C., Ruti, P. M. and co-authors. 1997. Validation of present-day regional climate simulations over Europe: LAM simulations with observed boundary conditions. *Clim. Dyn.* **13**, 489–506.

Christensen, O. B. and Christensen, J. H. 1998. Very high-resolution climate simulations over Scandinavia. *Present Climate. J. Climate* **11**(12), 3204–3229.

Christensen, J. H., Räisänen, J., Iversen, T., Bjørge, D., Christensen, O. B. and co-authors. 2001. A synthesis of regional climate change simulations – A Scandinavian perspective. *Geophys. Res. Lett.* **28**, 1003–1006.

Corti, S., Molteni, F. and Palmer, T. N., 1999. Signature of recent climate change in frequencies of natural atmospheric circulation regimes. *Nature* **398**, 799–802.

Denis, B., Laprise, R., Caya, D. and Coté, J. 2002. Downscaling ability of one-way nested regional climate models: the big-brother experiments. *Climate Dynam.* **18**, 627–646.

Engen-Skaugen, T., Haugen, J. E. and Tveito, O. E. 2007. Temperature scenarios for Norway: From regional to local scale. *Clim. Dynam.* **29**, 441–453.

Frogner, I.-L. and Iversen, T. 2002. High-resolution limited-area ensemble predictions based on low-resolution targeted singular vectors. *Q. J. R. Meteorol. Soc.* **128**, 1321–1341.

Furevik, T., Bentsen, M., Drange, H., Kindem, I. K. T., Kvamstø, G. and co-authors. 2003. Description and validation of the Bergen Climate Model: ARPEGE coupled with MICOM. *Clim. Dynam.* **21**, 27–51, doi:10.1007/s00382-003-0317-5.

Giorgi, F. and Mearns, L. O. 1991. Approaches to the simulation of regional climate change: A review. *Rev. Geophysics* **29**, 191–216.

Giorgi, F., Hewitson, B., Christensen, J., Hulme, M., von Storch, H. and co-authors. 2001. Regional climate information – evaluation and projections. In: *Climate Change 2001: The Scientific Basis* (EdsHoughton, J. T. *et al.*). Cambridge University Press, UK. 881 pp.

Gordon, C., Cooper, C., Senior, C. A., Banks, H., Gregory, J. M. and co-authors. 2000. The simulation of SST, sea ice extents and ocean heat transports in a version of the Hadley Centre coupled model without flux adjustments. *Clim. Dynam.* **16**, 147–166.

IPCC. 2001. *Climate Change 2001. The Scientific Basis*. (EdsHoughton, J. T. *et al.*). Cambridge University Press, UK. 881 pp.

IPCC. 2007. *Climate Change 2007: The Physical Science Basis. Summary for Policymakers*. Contribution of Working Group I to the Fourth Assessment Report of the Intergovernmental Panel on Climate Change. WMO, Geneva, Switzerland, 18 pp.

Iversen, T., Kristiansen, J., Jung, T. and Barkmeijer, J. 2008. Optimal atmospheric forcing perturbations for the cold ocean warm land pattern. *Tellus* **60A**, doi:10.1111/j.1600-0870.2008.00310.x

Jones, R. G., Murphy, J. M. and Noguer, M. 1995. Simulation of climate change over Europe using a nested regional-climate model. I: Assessment of control climate, including sensitivity to location of lateral boundaries. *Q. J. R. Meteorol. Soc.* **121**, 1413–1449.

Jones, R. G., Murphy, J. M., Noguer, M. and Keen, A. B. 1997. Simulations of climate change over Europe using a nested regional climate model. II: Comparison of driving and regional model responses to a doubling of carbon dioxide. *Q. J. R. Meteorol. Soc.* **123**, 265–292.

Jones, R., Hassell, D. and Murphy, J. 1999. *Configuring new climate models for Europe with improved climatologies via better representation of physical processes*. UKMO second year report for MERCURE, EC contract ENV4-CT97-0485.

Kanestrøm, I., Pedersen, K. and Skåtun, H. 1985. Major stationary ridges and troughs at 500mb. *Geophysica Norvegica* **33**, 1–40.

Kirkevåg, A., Iversen, T., Seland, Ø., Debernard, J. B., Kristjánsson, J. E. and co-authors. 2008. Aerosol-cloud-climate interactions in the climate model CAM-Oslo. *Tellus* **60A**, doi:10.1111/j.1600-0870.2008.00313.x.

Køltzow, M., Iversen, T. and Haugen, J. E., 2008. Extended Big-Brother experiments: The role of lateral boundary data quality and size of integration domain in regional climate modeling. *Tellus* **60A**, doi:10.1111/j.1600-0870.2008.00309.x.

McAveney, B. J., Covey, C., Joussaume, S., Kattsov, V., Kitoh, A. and co-authors. 2001. Model evaluation. In: *Climate Change 2001: The Scientific Basis* (Eds Houghton, J. T. *et al.*). Cambridge University Press, UK. 881 pp.

Nakicenovic, N., Alcamo, J., Davis, G., de Vries, B., Fenhann, J. and co-authors. 2000. *Special Report on Emissions Scenarios (SRES)*. Working Group III of the Intergovernmental Panel on Climate Change (IPCC), 595 pp. Cambridge University Press. (http://www.grida.no/climate/ipcc/emission/index.htm)

Palmer, T. N. and Räisänen, J. 2002. Quantifying risk of extreme seasonal precipitation events in a changing climate. *Nature* **415**, 512–514.

Räisänen, J. 2001. CO2-induced climate change in CMIP2 experiments; quantification of agreement and role of internal variability. *J. Climate* **14**, 2088–2104.

Räisänen, J. and Palmer, T. N. 2001. A probability and decision-model analysis of a multimodel ensemble of climate change simulations. *J. Climate* **14**, 3212–3226.

Räisänen, J., Hansson, U., Ullerstig, A., Doscher, R., Graham, L. P. and co-authors. 2004. European climate in the late twenty-first century: Regional simulations with two driving global models and two forcing scenarios. *Climate Dynam.* **22**, 13–31.

Rinke, A., Gerdes, R., K. Dethloff, T. Kandlbinder, M., Karcher, F. and co-authors. 2003. A case study of the anomalous Arctic sea ice conditions during 1990: Insights from coupled and uncoupled regional climate model simulations. *J. Geophys. Res.* **108**(D9), 4275, doi:10.1029/2002JD003146.

Roeckner, E., Arpe, K., Bengtsson, L., Christoph, M., Claussen, M. and co-authors. 1996. *The atmospheric general circulation model ECHAM4: model description and simulation of present-day climate: MPI Report 218*.

Roeckner, E., Bengtsson, L., Feichter, J., Lelieveld, J. and Rodhe, H. 1999. Transient climate change simulations with a coupled atmosphere-ocean GCM including the tropospheric sulfur cycle. *J. Climate* **12**, 3004–3032.

Seland, Ø., Iversen, T. and Kirkevåg, A. 2008. Sensitivity of aerosol climate interactions to basic assumptions in the CAM-Oslo atmospheric GCM. *Tellus* **60A**, in press.

Sorteberg, A., Furevik, T., Drange, H. and Kvamstø, N. G. 2005. Effects of simulated natural variability on Arctic temperature projections, *Geophys. Res. Lett.* **32**, L18708, doi:10.1029/2005GL023404.

Von Storch, H., Langenberg, H. and Feser, F. 2000. A spectral nudging technique for dynamical downscaling purposes, *Mon. Wea. Rev.* **128**, 3664–3672.

Wallace, J. M. and Gutzler, D. S., 1981. Teleconnections in the geopotential height field during the Northern Hemispheric winter. *Mon. Wea. Rev.* **109**, 784–812.

Wallace, J. M., Zhang, Y. and Bajuk, L. 1996. Interpretation of interdecadal trends in Northern Hemispheric surface air temperature. *J. Climate* **9**, 249–259.

Wilby, R. L. and Wigley, T. M. L. 1997. Downscaling general circulation model output; a review of methods and limitations. *Prog. Phys. Geogra.* **21**, 530–548.